Systems & Control Letters 219 (2027) 106642

Contents lists available at ScienceDirect

Systems & Control Letters

journal homepage: www.elsevier.com/locate/sysconle

Nonholonomic source seeking by torque tuning: Local and semi-global feedbacks

Bo Wang

Department of Mechanical Engineering, The City College of New York, The City University of New York, New York, NY 10031, USA

ARTICLE INFO

Keywords:
Source seeking
Averaging
Nonholonomic vehicles
Practical stability

ABSTRACT

This paper studies source seeking for a torque-controlled nonholonomic vehicle with a laterally displaced scalar sensor. The vehicle moves at a constant forward speed, while its yaw motion is controlled by torque with unknown inertia and damping. The objective is to steer the vehicle to a source-centered circular motion so that the lateral sensor approaches the unknown source, without using position, heading, source-location, gradient, or source-value information. The proposed torque law combines a fast oscillatory component, which generates averaged steering through symmetric product approximation, with a slowly tuned bias component that selects the desired orbit. Two bias-tuning designs are developed. The first is an output-feedback design using only the scalar measurement; it applies a Lie bracket extremum-seeking update and yields local practical convergence under a nested selection of the tuning parameters. The second is a velocity-assisted design using forward-speed and yaw-rate measurements; it tunes the bias through the yaw-rate tracking error and yields a globally asymptotically stable averaged system, implying semi-global practical stability of the original system. Simulations illustrate the proposed designs.

1. Introduction

Source seeking concerns the problem of steering a dynamical system toward the extremum of an unknown spatial signal using real-time measurements of the signal value [1–3]. This problem arises in applications such as locating chemical, thermal, electromagnetic, or acoustic sources, where the source position, signal gradient, and extremal value are not available a priori. Source-seeking techniques have been applied to diverse engineering systems, including autonomous vehicles [4,5], marine vessels [6], satellites [7], and particle accelerators [8]. In this paper, we consider source seeking for a torque-controlled nonholonomic vehicle moving in an unknown static scalar field. The vehicle is equipped with a scalar sensor that measures the signal value at the sensor location. The objective is to drive the vehicle toward the source, or equivalently to steer the vehicle toward a source-centered circular motion. Following the standard convention in extremum seeking, the source is treated as the unique minimum of the signal.

Velocity-level nonholonomic source seeking has been studied extensively for kinematic unicycle models, where the forward and angular velocities are treated as directly assignable control inputs. One line of work tuned the forward velocity while maintaining a constant angular velocity, using extremum seeking dithers to recover gradient information without position measurements [4,9,10]. A complementary line of work keeps the forward speed constant and tunes the angular velocity to steer the vehicle toward a source-centered orbit [11–13]. Source-seeking schemes that combine forward-speed regulation with steering control have been developed [14]. Related velocity-regulation ideas have also been developed for three-dimensional nonholonomic vehicles by tuning forward, pitch, and yaw velocities [15]. Stochastic excitation has also been used in nonholonomic source seeking [9], while more recent stochastic extremum-seeking methods have addressed distinct input delays [16]. Overall, the existing literature provides a mature velocity-level theory for nonholonomic source seeking, but does not address source seeking under force- or torque-actuated dynamics.

More recently, source seeking has been extended from velocity-level kinematic models to second-order dynamic models, where the inputs are forces or torques rather than velocities. This shift is natural for robotic vehicles, since inertia prevents instantaneous assignment of the forward or angular velocity. A key tool in this direction is the *symmetric product approximation* for mechanical systems under large-amplitude, high-frequency inputs [17]. This framework has enabled extremum- and source-seeking designs for force- and torque-actuated mechanical systems [18], including fully-actuated systems on Lie groups [19] and underactuated surface vessels [6]. In particular, [6] considers source seeking for strictly dissipative planar underactuated vehicles by surge-force tuning, using scalar measurements at the vehicle position. For nonholonomic vehicles, Suttner and Krstić developed force-actuated

E-mail address: bwang1@ccny.cuny.edu.

https://doi.org/10.1016/j.sysconle.2026.106642
Received 2 July 2026; Received in revised form 13 September 2026; Accepted 21 October 2026
0167-6911/© 2026 Elsevier B.V. All rights are reserved, including those for text and data mining, AI training, and similar technologies.

source-seeking laws for unicycles using symmetric product approximation [20,21]. They further extended this approach to torque-actuated nonholonomic source seeking, including planar unicycles and three-dimensional vehicles driven by pitch and yaw torque inputs [22,23]. Subsequent work addressed local extrema in dynamic-unicycle source seeking via circular sensing and divergence-theorem-based spatial averaging, with delayed measurements used in one design to extract nonlocal descent information [24,25]. The sensing configurations in these works are either collocated with the vehicle position [6,20,21,23,25] or forward-displaced along the vehicle heading [22,24].

The work most closely related to the present paper is [22], which proposed a source seeking law for a torque-controlled unicycle with a forward-displaced sensor. Their design uses a large-amplitude high-frequency torque input, and the symmetric product averaging analysis shows that the resulting averaged torque contains gradient-dependent steering information. Under suitable radial-symmetry and growth conditions, the averaged system admits a locally stable circular motion around the source. However, the radius of the limiting orbit is determined by physical and design parameters, and the sensor is not designed to converge to the source location. In contrast to the sensing configurations in [6,20–25], the present paper uses a *laterally displaced sensor* mounted perpendicular to the direction of forward motion and decomposes the yaw torque into a fast oscillatory component for averaged steering and a slowly tuned bias component for selecting the source-centered orbit. This structure makes the bias torque an explicit tuning target and leads to two designs with different sensing requirements: an output-feedback design using only scalar measurements and a velocity-assisted design using additional speed and yaw-rate measurements.

The main contributions of this paper are threefold. First, we introduce a torque-tuning framework for nonholonomic source seeking with a laterally displaced scalar sensor. The yaw torque is separated into a fast oscillatory component for averaged steering and a slowly tuned bias component for selecting the desired source-centered orbit. Second, we develop an output-feedback design that uses only the real-time scalar measurement. The bias is tuned through a Lie bracket extremum-seeking update applied to the steady response of the fast-averaged dynamics, yielding local practical convergence under a nested selection of the tuning parameters. Third, we develop a velocity-assisted design for the case where forward-speed and yaw-rate measurements are available. This design tunes the bias directly through the yaw-rate tracking error, yielding a globally asymptotically stable averaged system and semi-global practical uniform asymptotic stability of the original closed-loop system.

The remainder of the paper is organized as follows. Section 2 recalls the practical stability framework used in the analysis. Section 3 formulates the torque-controlled source seeking problem. Section 4 presents the two proposed torque-tuning designs and establishes their stability properties. Section 5 illustrates the designs through numerical simulations, and Section 6 concludes the paper.

2. Practical stability

This section reviews practical stability results for parameter-dependent systems from [26], which will be used in the subsequent analysis. For each $\varepsilon > 0$, let $f^\varepsilon : \mathbb{R}_{\geq 0} \times \mathbb{R}^n \to \mathbb{R}^n$ be a time-dependent vector field, and let $f : \mathbb{R}^n \to \mathbb{R}^n$ be an autonomous vector field. Consider two systems

$$\dot{x} = f^\varepsilon(t, x), \quad x(t_0) = x_0 \tag{1}$$

and

$$\dot{\bar{x}} = f(\bar{x}), \quad \bar{x}(t_0) = \bar{x}_0. \tag{2}$$

Assume that, for every $\varepsilon > 0$, $t_0 \geq 0$, and $x_0 \in \mathbb{R}^n$, (1) admits a unique maximal solution defined on $[t_0, \infty)$, and that the same holds for (2) for every $\bar{x}_0 \in \mathbb{R}^n$. For every $\varepsilon > 0$ and $t \geq 0$, let $\phi_t^\varepsilon : \mathbb{R}^n \to \mathbb{R}^n$ be a bijection. Along the solutions of (1), consider the time-dependent change of coordinates

$$\tilde{x} = \phi_t^\varepsilon(x). \tag{3}$$

The following definitions and result are adapted from [26].

Definition 1. We say that $x^\star \in \mathbb{R}^n$ is *semi-globally practically uniformly asymptotically stable for (1) in the variables (3)* if the following three properties hold.

(1) *Practical Uniform Stability.* For every $\eta > 0$, there exist $\delta > 0$ and $\varepsilon_0 > 0$ such that, for every $\varepsilon \in (0, \varepsilon_0]$, every $t_0 \geq 0$, and every $\tilde{x}_0 \in \mathbb{R}^n$ satisfying $|\tilde{x}_0 - x^\star| \leq \delta$, the maximal solution $x(t)$ of (1) with $x(t_0) = (\phi_{t_0}^\varepsilon)^{-1}(\tilde{x}_0)$ satisfies $|\phi_t^\varepsilon(x(t)) - x^\star| \leq \eta$ for all $t \geq t_0$.

(2) *Semi-Global Practical Uniform Boundedness.* For every $r > 0$, there exist $R > 0$ and $\varepsilon_0 > 0$ such that, for every $\varepsilon \in (0, \varepsilon_0]$, every $t_0 \geq 0$, and every $\tilde{x}_0 \in \mathbb{R}^n$ satisfying $|\tilde{x}_0 - x^\star| \leq r$, the maximal solution $x(t)$ of (1) with $x(t_0) = (\phi_{t_0}^\varepsilon)^{-1}(\tilde{x}_0)$ satisfies $|\phi_t^\varepsilon(x(t)) - x^\star| \leq R$ for all $t \geq t_0$.

(3) *Semi-Global Practical Uniform Attraction.* For every $r > 0$ and every $\eta > 0$, there exist $T > 0$ and $\varepsilon_0 > 0$ such that, for every $\varepsilon \in (0, \varepsilon_0]$, every $t_0 \geq 0$, and every $\tilde{x}_0 \in \mathbb{R}^n$ satisfying $|\tilde{x}_0 - x^\star| \leq r$, the maximal solution $x(t)$ of (1) with $x(t_0) = (\phi_{t_0}^\varepsilon)^{-1}(\tilde{x}_0)$ satisfies $|\phi_t^\varepsilon(x(t)) - x^\star| \leq \eta$ for all $t \geq t_0 + T$.

Definition 2. We say that *the solutions of (1) in the variables (3) approximate the solutions of (2)* if, for every compact set $K \subset \mathbb{R}^n$ and all $\eta, T > 0$, there exists $\varepsilon_0 > 0$ such that, for every $\varepsilon \in (0, \varepsilon_0]$, every $t_0 \geq 0$, and every $\bar{x}_0 \in K$, the following implication holds: If the solution $\bar{x}(t)$ of (2) with $\bar{x}(t_0) = \bar{x}_0$ satisfies $\bar{x}(t) \in K$ for all $t \in [t_0, t_0 + T]$, then the solution $x(t)$ of (1) with $x(t_0) = (\phi_{t_0}^\varepsilon)^{-1}(\bar{x}_0)$ satisfies $|\phi_t^\varepsilon(x(t)) - \bar{x}(t)| \leq \eta$ for all $t \in [t_0, t_0 + T]$.

Lemma 1. *Suppose that the solutions of (1) in the variables (3) approximate the solutions of (2). If $x^\star$ is a globally asymptotically stable equilibrium of (2), then $x^\star$ is semi-globally practically uniformly asymptotically stable for (1) in the variables (3).*

3. Problem statement

Consider a nonholonomic mobile robot moving in the plane. Let $(x, y) \in \mathbb{R}^2$ denote the position of the vehicle center in an inertial frame, let $\theta \in \mathbb{R}$ denote the heading angle, and let $\omega \in \mathbb{R}$ denote the yaw rate. The kinematics are

$$\dot{x} = v\cos\theta, \qquad \dot{y} = v\sin\theta, \qquad \dot{\theta} = \omega, \tag{4}$$

where the forward speed $v > 0$ is a constant maintained by a standard low-level velocity servo. The yaw dynamics are torque-actuated and given by

$$J\dot{\omega} = -d_\omega\omega + \tau, \tag{5}$$

where $\tau \in \mathbb{R}$ is the yaw torque input, $J > 0$ is the rotational inertia, and $d_\omega > 0$ is the yaw damping coefficient. The exact values of J and d_ω are unknown.

The vehicle moves in an unknown, static, radially symmetric scalar field

$$\Phi(x, y) = \psi\left((x - x^\star)^2 + (y - y^\star)^2\right), \tag{6}$$

where $(x^\star, y^\star) \in \mathbb{R}^2$ is the unknown source location. The radial profile is assumed to satisfy the following condition.

Assumption 1. The function $\psi : \mathbb{R}_{\geq 0} \to \mathbb{R}$ is twice continuously differentiable, satisfies $\psi'(s) > 0$ for all $s \geq 0$, and satisfies $\psi(s) \to \infty$ as $s \to \infty$.

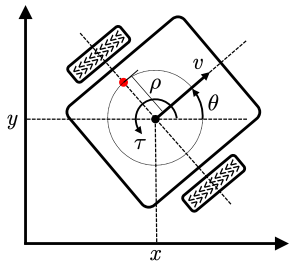


Fig. 1. Geometry of the torque-controlled nonholonomic vehicle with a left-side scalar sensor at lateral offset ρ.

Under Assumption 1, the scalar field Φ has a unique minimum at the source, where the minimum value $\Phi(x^\star, y^\star) = \psi(0)$ is unknown. The task of the vehicle is to seek the minimum point of the scalar field.

A scalar sensor is mounted on the left side of the vehicle at a lateral offset $\rho > 0$, as shown in Fig. 1. Define the position error vector in the body frame by

$$\begin{bmatrix} x_e \\ y_e \end{bmatrix} := \begin{bmatrix} \cos\theta & \sin\theta \\ -\sin\theta & \cos\theta \end{bmatrix} \begin{bmatrix} x - x^\star \\ y - y^\star \end{bmatrix}. \tag{7}$$

Hence, the value of the signal function ψ at the position of the sensor is

$$\mathsf{y}_\mathsf{m} = \psi(s), \quad s := x_e^2 + (y_e + \rho)^2. \tag{8}$$

The control objective is to design yaw torque laws using the real-time scalar measurement $\mathsf{y}_\mathsf{m}(t)$ such that the closed-loop vehicle approaches the source-centered circular motion. Measurements of the configuration variables x, y or θ are not available. The desired motion is characterized by $(x_e, y_e, \omega) = (0, -\rho, v/\rho)$. At this motion, the vehicle travels on a circle of radius ρ centered at the source, and the left-side sensor is located at the source, so $s = 0$ and $\mathsf{y}_\mathsf{m} = \Phi(x^\star, y^\star)$.

4. Control designs and main results

This section presents two control designs with different sensing requirements. The first uses only the real-time scalar measurement $\mathsf{y}_\mathsf{m}(t)$ and combines a fast symmetric product torque excitation with a slow Lie bracket bias update, yielding local practical convergence. The second additionally uses measurements of v and ω to shape the yaw-rate tracking error directly, yielding a globally asymptotically stable averaged system and a semi-global practical stability result for the original system. The block diagrams of the two proposed designs are illustrated in Fig. 2. Together, the two designs quantify the tradeoff between sensing capability and guaranteed stability region.

4.1. Local output-feedback design

Let $u_1, u_2 : \mathbb{R}_{\geq 0} \to \mathbb{R}$ be bounded, piecewise continuous, zero-mean, T-periodic functions. We assume that u_1 and u_2 are normalized as

$$\frac{1}{T}\int_0^T u_2(\sigma)\int_0^\sigma u_1(\xi)\mathrm{d}\xi\mathrm{d}\sigma = \frac{1}{2}. \tag{9}$$

Let $w : \mathbb{R}_{\geq 0} \to \mathbb{R}$ be a bounded, nonzero, piecewise continuous, zero-mean, T_w-periodic function. Let W denote the T_w-periodic zero-mean antiderivative of w, i.e., $W' = w$. We assume that w is scaled so that

$$\frac{1}{T_w}\int_0^{T_w} W^2(\sigma)\mathrm{d}\sigma = \frac{1}{2}. \tag{10}$$

Define the nominal steady-state yaw torque required to sustain the desired circular motion as

$$\mu^\star := \frac{d_\omega v}{\rho}. \tag{11}$$

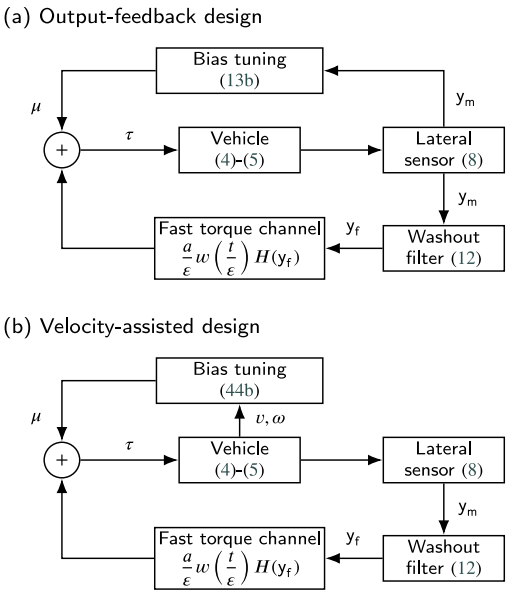


Fig. 2. Block diagrams of the two proposed torque-tuning designs: (a) output-feedback and (b) velocity-assisted.

Since $\mu^\star > 0$, for the analysis below, let $\mathcal{I} \subset (0, \infty)$ be any compact interval such that $\mu^\star \in \mathrm{Int}(\mathcal{I})$. The interval $\mathcal{I}$ is introduced only as an analytical neighborhood of $\mu^\star$ and is not required for controller implementation.

The scalar measurement y_m is first passed through the washout filter

$$\dot{z} = -\lambda z + \lambda \mathsf{y}_\mathsf{m}, \qquad \mathsf{y}_\mathsf{f} = \mathsf{y}_\mathsf{m} - z, \tag{12}$$

where $\lambda > 0$. We propose the output-feedback control law

$$\tau = \mu + \frac{a}{\varepsilon} w\left(\frac{t}{\varepsilon}\right) H(\mathsf{y}_\mathsf{f}), \tag{13a}$$

$$\dot{\mu} = \frac{b\Omega}{\sqrt{\delta}}\left[u_1\left(\frac{\Omega t}{\delta}\right)\sin(\mathsf{y}_\mathsf{m}) + u_2\left(\frac{\Omega t}{\delta}\right)\cos(\mathsf{y}_\mathsf{m})\right], \tag{13b}$$

where $a > 0$ and $b > 0$ are control gains; $\varepsilon > 0$ determines the time scale of the fast torque excitation; $\Omega > 0$ determines the time scale of the slow bias evolution; and $\delta > 0$ determines the frequency of the bias dither on the slow time scale Ωt. The parameters δ, Ω, and ε will be selected successively in the stability analysis. The variable μ is the slowly varying yaw-torque bias. The shaping function $H : \mathbb{R} \to \mathbb{R}$ satisfies $H \in C^2(\mathbb{R})$ and

$$\Gamma(q) := H(q)H'(q) > 0, \quad \Gamma'(q) > 0, \quad \forall q \in \mathbb{R}. \tag{14}$$

For example, (14) is satisfied by the exponential family $H(q) = \alpha e^{\beta q}$, with $\alpha, \beta > 0$, as well as by the choice $H(q) = q + \sqrt{q^2 + 1}$. As shown in the analysis below, H enters the averaged steering action through $\Gamma = HH'$; hence, its choice affects the transient convergence behavior. The control law (12)–(13) is output feedback: it uses the scalar measurement y_m only, together with the internally generated filter and bias state.

For analysis, define

$$r := v - \rho\omega. \tag{15}$$

Then, the closed-loop system can be written in the analysis coordinates (x_e, y_e, r, z, μ) as

$$\dot{x}_e = r + \omega(y_e + \rho), \tag{16a}$$

$$\dot{y}_e = -\omega x_e, \tag{16b}$$

$$\dot{r} = -\frac{d_\omega}{J} r - \frac{\rho}{J}\left[\mu - \mu^\star + \frac{a}{\varepsilon} w\left(\frac{t}{\varepsilon}\right) H(\mathsf{y}_\mathsf{f})\right], \tag{16c}$$

$$\dot{z} = -\lambda z + \lambda\psi(s), \tag{16d}$$

$$\dot{\mu} = \frac{b\Omega}{\sqrt{\delta}}\left[u_1\left(\frac{\Omega t}{\delta}\right)\sin(\mathrm{y_m}) + u_2\left(\frac{\Omega t}{\delta}\right)\cos(\mathrm{y_m})\right], \tag{16e}$$

where $\omega = (v - r)/\rho$, $s = x_e^2 + (y_e + \rho)^2$, and $\mathrm{y_f} = \psi(s) - z$.

The closed-loop system (16) involves several separated time scales. The torque excitation $w(t/\varepsilon)$ has period $O(\varepsilon)$ and induces a fast oscillatory response in the yaw dynamics, while the underlying plant and filter dynamics evolve on the $O(1)$ time scale. The bias update contains the periodic signals $u_i(\Omega t/\delta)$, whose period is $O(\delta/\Omega)$ in the original time t. Its averaged evolution, derived below, occurs on the slower $O(1/\Omega)$ time scale. Equivalently, on the slow time $\sigma = \Omega t$, the bias dither has period $O(\delta)$, whereas the averaged bias dynamics evolve on the $O(1)$ time scale. Thus, δ controls the Lie bracket averaging of the bias update, while Ω separates the bias dynamics from the plant/filter dynamics. This structure motivates the two-stage averaging analysis below. For fixed δ and Ω, the bias μ is treated as frozen during the $O(\varepsilon)$ fast-torque averaging, since its variation over one excitation period vanishes as $\varepsilon \to 0$. The resulting fast-torque-averaged dynamics define, locally, a quasi-steady-state branch parameterized by μ. The bias update is then analyzed on the slow time $\sigma = \Omega t$ through the corresponding steady input–output map. The precise nested selection of δ, Ω, and ε is stated in Theorem 1.

For analysis, define the change of variables by

$$\tilde{x}_e = x_e, \quad \tilde{y}_e = y_e, \quad \tilde{z} = z, \quad \tilde{\mu} = \mu \tag{17a}$$

$$\tilde{r} = r + \frac{\rho a}{J} W\left(\frac{t}{\varepsilon}\right) H(\psi(s) - z). \tag{17b}$$

Although (17) contains the unknown inertia J, it is introduced solely for analysis and is not required for controller implementation; in particular, the proposed control laws do not require knowledge of J.

4.1.1. Fast averaging via symmetric product approximation

In the first step of the analysis, we average the closed-loop system (16) on the fast time scale using the *symmetric product approximation*[1] for the yaw-torque channel [17]. During this fast averaging calculation, the controller states z and μ are treated as frozen parameters.

The relevant mechanical channel for the fast averaging is the one-dimensional yaw dynamics

$$\nabla_{\dot{\theta}}\dot{\theta} = Y_0(\dot{\theta}) + \frac{a}{\varepsilon} w\left(\frac{t}{\varepsilon}\right) Y_1(\theta), \tag{18}$$

where

$$Y_0(\dot{\theta}) := \left(-\frac{d_\omega}{J}\dot{\theta} + \frac{\mu}{J}\right)\frac{\partial}{\partial\theta}, \quad Y_1(\theta) := \frac{1}{J} H(\psi(s) - z)\frac{\partial}{\partial\theta},$$

and ∇ is the trivial affine connection on $\mathbb{R}$. Strictly speaking, Y_1 also depends on the frozen parameters x, y, and z through $s = x_e^2 + (y_e + \rho)^2$; this dependence is suppressed for notational simplicity, while the dependence of s on θ is retained in the symmetric product calculation.

Equivalently, in the yaw rate coordinate, (17) gives

$$\tilde{\omega} = \omega - \frac{a}{J} W\left(\frac{t}{\varepsilon}\right) H(\psi(s) - z). \tag{19}$$

For fixed values of the frozen parameters, following [17], the solutions of (18) in the variables (19) approximate the solutions of

$$\nabla_{\dot{\bar{\theta}}}\dot{\bar{\theta}} = Y_0(\dot{\bar{\theta}}) - \frac{a^2}{4}\langle Y_1 : Y_1\rangle(\bar{\theta}), \tag{20}$$

where $\langle Y_1 : Y_1\rangle$ is the symmetric product given by $\langle Y_1 : Y_1\rangle := 2\nabla_{Y_1} Y_1$. Since the connection is trivial, direct calculation yields

$$\nabla_{Y_1} Y_1(\theta) = \frac{1}{J^2} H(\mathrm{y_f}) H'(\mathrm{y_f}) \frac{\partial \mathrm{y_f}}{\partial\theta}\frac{\partial}{\partial\theta}.$$

[1] After lifting the second-order mechanical dynamics to the tangent bundle, the symmetric product terms can equivalently be represented through iterated Lie brackets. We retain the terminology "symmetric product approximation" to emphasize the second-order mechanical formulation, in which the averaged effect is naturally expressed in terms of symmetric products.

Hence, using $\partial \mathrm{y_f}/\partial\theta = -2\rho\psi'(s)x_e$, (20) becomes

$$J\dot{\bar{\omega}} = -d_\omega\bar{\omega} + \mu + \frac{a^2\rho}{J}\Gamma(\bar{\mathrm{y}}_\mathrm{f})\psi'(\bar{s})\bar{x}_e, \tag{21}$$

where $\bar{s} := \bar{x}_e^2 + (\bar{y}_e + \rho)^2$ and $\bar{\mathrm{y}}_\mathrm{f} := \psi(\bar{s}) - \bar{z}$.

With the definition $\bar{r} := v - \rho\bar{\omega}$, one has $\dot{\bar{r}} = -\rho\dot{\bar{\omega}}$. Hence, for each fixed bias μ, the associated fixed-bias fast-averaged system is

$$\dot{\bar{x}}_e = \bar{r} + \bar{\omega}(\bar{y}_e + \rho), \tag{22a}$$

$$\dot{\bar{y}}_e = -\bar{\omega}\bar{x}_e, \tag{22b}$$

$$\dot{\bar{r}} = -\frac{d_\omega}{J}\bar{r} - \frac{\rho}{J}(\mu - \mu^\star) - \frac{a^2\rho^2}{J^2}\Gamma(\bar{\mathrm{y}}_\mathrm{f})\psi'(\bar{s})\bar{x}_e, \tag{22c}$$

$$\dot{\bar{z}} = -\lambda\bar{z} + \lambda\psi(\bar{s}), \tag{22d}$$

where $\bar{\omega} = (v - \bar{r})/\rho$. For each fixed $\mu \in \mathrm{Int}(\mathcal{I})$, the fast-averaged system (22) has the unique equilibrium

$$\bar{x}_{e*} = 0, \ \bar{y}_{e*} = -\frac{\rho\mu^\star}{\mu}, \ \bar{r}_* = -\frac{\rho}{d_\omega}(\mu - \mu^\star), \ \bar{z}_* = \psi(\bar{s}_*), \tag{23}$$

where

$$\bar{s}_*(\mu) = \bar{x}_{e*}^2 + \left(\bar{y}_{e*} + \rho\right)^2 = \rho^2\left(1 - \frac{\mu^\star}{\mu}\right)^2.$$

Proposition 1. *Suppose that Assumption 1 holds. Then, for each fixed $\mu \in \mathrm{Int}(\mathcal{I})$, the equilibrium (23) of (22) is locally exponentially stable. Moreover, there exists a compact interval contained in $\mathrm{Int}(\mathcal{I})$ and containing $\mu^\star$ in its interior such that the equilibrium family is uniformly locally exponentially stable for all μ in this interval.*

Proof. Fix $\mu \in \mathrm{Int}(\mathcal{I})$ and introduce the local linearization coordinates $\chi := \mathrm{col}\left(\bar{x}_e - \bar{x}_{e*}, \bar{y}_e - \bar{y}_{e*}, \bar{r} - \bar{r}_*, \bar{z} - \bar{z}_*\right)$. At the equilibrium (23), one has $\bar{\omega}_* = \mu/d_\omega$ and $\bar{\mathrm{y}}_{\mathrm{f}*} = \psi(\bar{s}_*) - \bar{z}_* = 0$. Linearizing (22) about the equilibrium (23) gives $\dot{\chi} = A_\mu\chi$, where

$$A_\mu = \begin{bmatrix} 0 & \frac{\mu}{d_\omega} & \frac{\mu^\star}{\mu} & 0 \\ -\frac{\mu}{d_\omega} & 0 & 0 & 0 \\ -\frac{a^2\rho^2}{J^2}\Gamma(0)\psi'(\bar{s}_*) & 0 & -\frac{d_\omega}{J} & 0 \\ 0 & 2\lambda\psi'(\bar{s}_*)(\bar{y}_{e*} + \rho) & 0 & -\lambda \end{bmatrix}.$$

The characteristic polynomial of A_μ is

$$\det(\zeta I - A_\mu) = (\zeta + \lambda)\left[\zeta^3 + c_2\zeta^2 + c_1\zeta + c_0\right], \tag{24}$$

where $c_2 := d_\omega/J > 0$, $c_0 := \mu^2/(Jd_\omega) > 0$, and $c_1 := (\mu/d_\omega)^2 + (\mu^\star/\mu)(a^2\rho^2/J^2)\Gamma(0)\psi'(\bar{s}_*) > 0$. Moreover, $c_2c_1 - c_0 = d_\omega\mu^\star a^2\rho^2\Gamma(0)\psi'(\bar{s}_*)/(\mu J^3) > 0$. Hence, by the Routh–Hurwitz criterion for cubic polynomials, all roots of $\zeta^3 + c_2\zeta^2 + c_1\zeta + c_0$ have negative real parts. The remaining eigenvalue is $-\lambda < 0$. Therefore A_μ is Hurwitz, and the linearization theorem implies that the equilibrium (23) is locally exponentially stable.

Finally, A_μ depends continuously on μ. Since $A_{\mu^\star}$ is Hurwitz, there exists a compact interval contained in $\mathrm{Int}(\mathcal{I})$ and containing $\mu^\star$ in its interior on which the eigenvalues of A_μ are uniformly bounded away from the imaginary axis. Together with the C^1 dependence of (22) and (23) on μ, the standard uniform linearization argument gives uniform local exponential stability of the equilibrium family on this interval [27, Section 11.2]. □

For notational simplicity, denote

$$\xi := (\bar{x}_e, \bar{y}_e, \bar{r}, \bar{z}), \tag{25}$$

and let $f_\xi(\xi, \mu)$ denote the right-hand side of (22). The equilibrium in (23) is denoted by $\xi_*(\mu)$. The system (22) was obtained by freezing the slowly varying bias μ during the fast torque averaging. Restoring

the bias update after this averaging step gives the fast-torque-averaged system

$$\dot{\xi} = f_\xi(\xi, \mu), \tag{26a}$$

$$\dot{\mu} = \frac{b\Omega}{\sqrt{\delta}}\left[u_1\left(\frac{\Omega t}{\delta}\right)\sin\big(\psi(\bar{s})\big) + u_2\left(\frac{\Omega t}{\delta}\right)\cos\big(\psi(\bar{s})\big)\right], \tag{26b}$$

where $\bar{s} = \bar{x}_e^2 + (\bar{y}_e + \rho)^2$. Thus, Proposition 1 characterizes the fixed-μ subsystem of (26), while the second equation retains the oscillatory bias-tuning dynamics. For fixed δ and Ω, the symmetric product approximation extends to the full transformed closed-loop system, with z and μ included as additional slow states. Hence, on compact sets and finite time intervals, the solutions of (16) in the variables (17) approach those of (26) uniformly as $\varepsilon \to 0$ [17].

4.1.2. Slow bias averaging via Lie bracket approximation

Next, we analyze the slow bias dynamics of the fast-torque-averaged system (26). By Proposition 1, the fixed-μ subsystem admits a locally exponentially stable equilibrium branch $\xi_*(\mu)$. Restricting (26) to the quasi-steady-state branch $\xi = \xi_*(\mu)$ defines a steady input–output map from the yaw-torque bias μ to the corresponding scalar measurement. Define this map by

$$P : \mathcal{I} \to \mathbb{R}, \qquad P(\mu) := \psi\left(\bar{s}_*(\mu)\right). \tag{27}$$

Differentiating P gives

$$P'(\mu) = p(\mu)(\mu - \mu^\star), \quad p(\mu) := \frac{2\rho^2\mu^\star}{\mu^3}\psi'(\bar{s}_*(\mu)). \tag{28}$$

Since $\mathcal{I} \subset (0, \infty)$ is compact, $\mu^\star > 0$, and $\psi'(s) > 0$, one has $\underline{p} := \min_{\mu\in\mathcal{I}} p(\mu) > 0$, and therefore

$$(\mu - \mu^\star)P'(\mu) \geq \underline{p}(\mu - \mu^\star)^2, \qquad \forall\, \mu \in \mathcal{I}. \tag{29}$$

Thus, $\mu^\star$ is the unique minimizer of P on $\mathcal{I}$, and the descent direction $-P'(\mu)$ points toward $\mu^\star$.

Let $\sigma := \Omega t$. On the quasi-steady-state branch $\xi = \xi_*(\mu)$, the fast-torque-averaged system reduces to

$$\frac{\mathrm{d}\mu}{\mathrm{d}\sigma} = \frac{b}{\sqrt{\delta}}\left[u_1\left(\frac{\sigma}{\delta}\right)\sin(P(\mu)) + u_2\left(\frac{\sigma}{\delta}\right)\cos(P(\mu))\right]. \tag{30}$$

Using the normalization (9) and following [13,28], the corresponding Lie bracket averaged dynamics are

$$\frac{\mathrm{d}\bar{\mu}}{\mathrm{d}\sigma} = \frac{b^2}{2}[g_1, g_2](\bar{\mu}) = -\frac{b^2}{2}P'(\bar{\mu}), \tag{31}$$

where $g_1(\mu) := \sin(P(\mu))$ and $g_2(\mu) := \cos(P(\mu))$. Equivalently, in the original time variable,

$$\dot{\bar{\mu}} = -\frac{b^2\Omega}{2}P'(\bar{\mu}). \tag{32}$$

The averaged bias dynamics (32) are a gradient descent for P. For $V_\mu := \frac{1}{2}(\bar{\mu} - \mu^\star)^2$, (29) and (32) give

$$\dot{V}_\mu = -\frac{b^2\Omega}{2}(\bar{\mu} - \mu^\star)P'(\bar{\mu}) \leq -\frac{b^2\Omega}{2}\underline{p}(\bar{\mu} - \mu^\star)^2. \tag{33}$$

Hence,

$$|\bar{\mu}(t) - \mu^\star| \leq |\bar{\mu}(t_0) - \mu^\star| \exp\left(-\frac{b^2\underline{p}}{2}\Omega(t - t_0)\right), \tag{34}$$

which explicitly shows that the convergence rate of the averaged bias dynamics is proportional to Ω.

4.1.3. Stability analysis

Combining (22) with (32) gives the fully averaged system

$$\dot{\xi} = f_\xi(\xi, \bar{\mu}), \tag{35a}$$

$$\dot{\bar{\mu}} = -\Omega k_\mu P'(\bar{\mu}), \tag{35b}$$

where $k_\mu := b^2/2$. The equilibrium of (35) is given by

$$(\xi^\star, \mu^\star) := (0, -\rho, 0, \psi(0), \mu^\star). \tag{36}$$

Proposition 2. *Suppose that Assumption 1 holds. Then there exists $\Omega_0 > 0$ such that, for every $\Omega \in (0, \Omega_0]$, the equilibrium $(\xi^\star, \mu^\star)$ of (35) is locally asymptotically stable.*

Proof. In the slow time $\sigma := \Omega t$, (35) can be written in the standard singularly perturbed form [27]. By Proposition 1, the boundary-layer equilibrium branch $\xi_*(\bar{\mu})$ is uniformly locally exponentially stable for $\bar{\mu}$ in a compact interval containing $\mu^\star$ in its interior. The reduced system (35b) is obtained by setting $\xi = \xi_*(\bar{\mu})$. Following (33), $\mu^\star$ is a locally exponentially stable equilibrium of the reduced system. The conclusion follows from the standard singular perturbation theorem on the infinite time interval [27, Theorem 11.4]. □

Proposition 2 characterizes the limiting behavior of the fully averaged system (35). For the original closed-loop system, however, the oscillatory bias dynamics in the fast-torque-averaged system (26) must be retained, and the effects of δ, Ω, and ε must be accounted for separately. The framework in Section 2 is formulated for a single perturbation parameter, whereas the output-feedback design involves the nested parameters δ, Ω, and ε. We therefore state the following theorem directly in terms of their ordered selection and the resulting practical convergence estimates.

Theorem 1. *Suppose Assumption 1 holds and choose the shaping function H such that (14) is satisfied. Let $\tilde{\xi} := (\tilde{x}_e, \tilde{y}_e, \tilde{r}, \tilde{z})$. Then there exist $r_\mu, r_\xi > 0$ and $\beta_\mu, \beta_\xi \in \mathcal{KL}$ such that the following holds. For every $\nu > 0$, there exists $\delta_0 > 0$ such that, for every $\delta \in (0, \delta_0]$, there exists $\Omega_0(\delta, \nu) > 0$ such that, for every $\Omega \in (0, \Omega_0]$, there exists $\varepsilon_0(\delta, \Omega, \nu) > 0$ such that, for every $\varepsilon \in (0, \varepsilon_0]$, every $t_0 \geq 0$, and every initial condition satisfying*

$$|\mu(t_0) - \mu^\star| \leq r_\mu, \quad |\tilde{\xi}(t_0) - \xi_*(\mu(t_0))| \leq r_\xi,$$

the solution of (16) is defined for all $t \geq t_0$ and satisfies

$$|\mu(t) - \mu^\star| \leq \beta_\mu\big(|\mu(t_0) - \mu^\star|, \Omega(t - t_0)\big) + \nu, \tag{37a}$$

$$|\tilde{\xi}(t) - \xi_*(\mu(t))| \leq \beta_\xi\big(|\tilde{\xi}(t_0) - \xi_*(\mu(t_0))|, t - t_0\big) + \nu. \tag{37b}$$

Since $\xi_*(\mu)$ is locally Lipschitz and $\xi_*(\mu^\star) = \xi^\star$, (37) implies practical convergence to the target point $(\xi^\star, \mu^\star)$.

Proof. The proof follows the same decomposition as the argument in [13, Theorem 7], but all steps are carried out locally. Choose $r_\mu > 0$ sufficiently small so that $|\mu - \mu^\star| \leq 2r_\mu$ lies in the compact interval of Proposition 1, and choose $r_\xi > 0$ within the corresponding uniform exponential stability neighborhood. Since $\xi_*(\mu)$ is continuously differentiable on this interval, there exists $L_* > 0$ such that $|\xi_*(\mu_1) - \xi_*(\mu_2)| \leq L_*|\mu_1 - \mu_2|$. Let $\hat{\nu} > 0$ be sufficiently small relative to ν, r_μ, and r_ξ.

We first consider the reduced bias dynamics (30). The associated Lie bracket system is (31), and (34) gives

$$|\bar{\mu}(\sigma) - \mu^\star| \leq \beta_\mu(|\bar{\mu}(\sigma_0) - \mu^\star|, \sigma - \sigma_0), \tag{38}$$

where $\beta_\mu(r, s) := r\exp(-b^2\underline{p}s/2)$. On the compact interval under consideration, the assumptions of the Lie bracket approximation results in [28] are satisfied. By [28, Theorem 2], $\mu^\star$ is locally practically uniformly asymptotically stable for (30). Combining this practical stability with the finite-time trajectory approximation of [28, Theorem 1], $\delta_0 > 0$ can be chosen so that, for every $\delta \in (0, \delta_0]$ and every solution μ_r with $|\mu_\mathrm{r}(t_0) - \mu^\star| \leq r_\mu$,

$$|\mu_\mathrm{r}(t) - \mu^\star| \leq \beta_\mu(|\mu_\mathrm{r}(t_0) - \mu^\star|, \Omega(t - t_0)) + \hat{\nu}, \quad t \geq t_0. \tag{39}$$

Indeed, finite-time approximation gives this estimate up to a settling time, while practical uniform attraction and stability keep the trajectory within the $\hat{\nu}$-neighborhood thereafter.

We next consider the fast-torque-averaged system (26) and set $e := \xi - \xi_*(\mu)$. Uniform local exponential stability in Proposition 1 and the converse Lyapunov theorem give constants $c_\xi, \lambda_\xi, C_\xi > 0$, independent

of μ on the chosen interval, such that, as long as the trajectory remains in the above neighborhood,

$$|e(t)| \le c_\xi e^{-\lambda_\xi (t-t_0)}|e(t_0)| + C_\xi \sup_{s\in[t_0,t]} |\dot\mu(s)|. \tag{40}$$

Since the periodic inputs are bounded, $|\dot\mu| \le C\Omega/\sqrt{\delta}$ for some $C > 0$. Thus, for each fixed δ, Ω can be chosen sufficiently small so that

$$|e(t)| \le \beta_\xi(|e(t_0)|, t-t_0) + \hat\nu, \tag{41}$$

where $\beta_\xi(r,s) := c_\xi r\exp(-\lambda_\xi s)$. It remains to compare the bias component of (26) with (30). For fixed δ, (26) is a singularly perturbed system in the slow time $\sigma = \Omega t$, with boundary-layer equilibrium $\xi_*(\mu)$ and reduced system (30). Choose $S_\nu > 0$ so that $\beta_\mu(r_\mu, S_\nu) \le \hat\nu$. By the finite-interval singular perturbation theorem, $\Omega_0(\delta,\nu) > 0$ can be chosen so that

$$|\mu(t) - \mu_{\mathrm{r}}(t)| \le \hat\nu, \quad \Omega(t-t_0) \in [0, S_\nu]. \tag{42}$$

To justify that the local estimates remain valid, suppose that a first exit from $|\mu-\mu^\star| < 2r_\mu$, $|e| < 2r_\xi$ occurs before the end of this interval. Eqs. (39), (41), and (42), with $\hat\nu$ chosen sufficiently small, place the trajectory strictly inside these bounds, contradicting the definition of the first exit. Hence the estimates hold throughout the interval.

At $\Omega(t-t_0) = S_\nu$, the trajectory lies in a smaller practical tube. Practical stability of (30), together with (41) and the same finite-interval singular perturbation estimate, shows by continuation that this larger tube is forward invariant. This continuation is used only after the settling time; the $\mathcal{KL}$ transient is the one obtained on the initial interval. Consequently, after reducing $\hat\nu$ if necessary,

$$|\mu(t)-\mu^\star| \le \beta_\mu(|\mu(t_0)-\mu^\star|, \Omega(t-t_0)) + \frac{\nu}{4},$$
$$|\xi(t) - \xi_*(\mu(t))| \le \beta_\xi(|\xi(t_0)-\xi_*(\mu(t_0))|, t-t_0) + \frac{\nu}{4}$$

for all $t \ge t_0$.

We finally return to the original closed-loop system. Temporarily denote its transformed trajectory by $(\tilde\xi^\varepsilon, \mu^\varepsilon)$ and let (ξ,μ) be the solution of (26) with matching initial conditions. Fix δ and Ω as above and choose $T_\nu > 0$ such that $\beta_\mu(r_\mu, \Omega T_\nu) \le \nu/4$ and $\beta_\xi(r_\xi, T_\nu) \le \nu/4$. By the symmetric product approximation stated after (26), $\varepsilon_0(\delta,\Omega,\nu) > 0$ can be chosen so that

$$|\tilde\xi^\varepsilon(t) - \xi(t)| + |\mu^\varepsilon(t) - \mu(t)| \le \frac{\nu}{4(1+L_*)} \tag{43}$$

for all $t \in [t_0, t_0+T_\nu]$. Combining the above estimations and (43) yields (37a)–(37b) on $[t_0, t_0+T_\nu]$. At $t = t_0+T_\nu$, the transformed trajectory lies in a smaller practical tube. The practical stability established above for (26), together with the uniform finite-time symmetric product approximation, gives, by the same first-exit/continuation argument, that the original transformed trajectory remains in the prescribed larger tube for all $t \ge t_0 + T_\nu$. No restarted $\mathcal{KL}$ estimate is used after this settling time. Since the $\mathcal{KL}$ terms are nonnegative, (37a)–(37b) therefore hold for all $t \ge t_0$.

Finally, local Lipschitz continuity of ξ_* gives $|\tilde\xi(t) - \xi^\star| \le \beta_\xi(|\tilde\xi(t_0) - \xi_*(\mu(t_0))|, t-t_0) + L_*\beta_\mu(|\mu(t_0)-\mu^\star|, \Omega(t-t_0)) + (1+L_*)\nu$, which proves practical convergence to $(\xi^\star,\mu^\star)$. □

Remark 1. The output-feedback design is not a minor modification of the torque law in [22]. In [22], the torque consists only of a large-amplitude oscillatory term, and the limiting circular orbit is determined implicitly by the balance among the physical parameters, the design gains, and the averaged gradient-dependent torque. In the present design, the yaw torque contains an additional slowly varying bias. This bias is not merely an offset; it is the quantity to be tuned so that the desired source-centered orbit is selected. The lateral sensor placement is also essential. Instead of placing the sensor in front of the vehicle, the sensor is placed on the side, so that the desired circular motion corresponds to the sensor being located at the source. Thus, the scalar measurement provides information for tuning the bias toward the source-centered orbit. With only the scalar measurement, this tuning is achieved indirectly through a Lie bracket extremum-seeking update, which leads to a local practical convergence result.

4.2. Semi-global velocity-assisted design

The preceding design uses only the scalar measurement $\mathsf{y}_{\mathsf{m}}(t)$. In many robotic platforms, however, the forward speed $v(t)$ and yaw rate $\omega(t)$ are readily available from wheel, motor, or inertial sensors. The following design uses this additional velocity information to tune the bias torque; it still does not require measurements of the vehicle position, heading, source location, field gradient, inertia, or damping coefficient.

We keep the washout filter (12) and the same fast torque excitation, but replace the Lie bracket bias update with the yaw-rate tracking feedback

$$\tau = \mu + \frac{a}{\varepsilon} w\left(\frac{t}{\varepsilon}\right) H(\mathsf{y}_{\mathsf{f}}), \tag{44a}$$
$$\dot\mu = k(v - \rho\omega), \tag{44b}$$

where $a > 0$ and $k > 0$ are control gains. Then, the closed-loop system can be written in the analysis coordinates (x_e, y_e, r, z, μ) as

$$\dot x_e = r + \omega(y_e + \rho), \tag{45a}$$
$$\dot y_e = -\omega x_e, \tag{45b}$$
$$\dot r = -\frac{d_\omega}{J} r - \frac{\rho}{J}\left[\mu - \mu^\star + \frac{a}{\varepsilon} w\left(\frac{t}{\varepsilon}\right) H(\mathsf{y}_{\mathsf{f}})\right], \tag{45c}$$
$$\dot z = -\lambda z + \lambda\psi(s), \tag{45d}$$
$$\dot\mu = kr, \tag{45e}$$

After the same symmetric product averaging step as in the previous subsection, the averaged system is

$$\dot{\bar\xi} = f_{\bar\xi}(\bar\xi, \bar\mu) \tag{46a}$$
$$\dot{\bar\mu} = k\bar r. \tag{46b}$$

The equilibrium of (46) is given by (36).

Proposition 3. *Suppose Assumption 1 holds. Then the equilibrium $(\xi^\star,\mu^\star)$ is globally asymptotically stable for (46).*

Proof. Let $\kappa := a^2\rho^2/J^2$. Consider

$$V := \frac{1}{2}\bar r^2 + \frac{\kappa\Gamma(0)}{2}\big(\psi(\bar s) - \psi(0)\big) + \frac{\kappa}{2}\int_0^{\bar{\mathsf{y}}_{\mathsf{f}}} (\Gamma(\zeta) - \Gamma(0))\,\mathrm{d}\zeta + \frac{\rho}{2Jk}(\bar\mu - \mu^\star)^2. \tag{47}$$

Since $\psi'(s) > 0$ and $\Gamma'(\zeta) > 0$, V is positive definite with respect to $(\xi^\star,\mu^\star)$ and radially unbounded. Differentiating V along (46) and using $\dot{\bar s} = 2\bar x_e\bar r$ and $\dot{\bar{\mathsf{y}}}_{\mathsf{f}} = 2\psi'(\bar s)\bar x_e\bar r - \lambda\bar{\mathsf{y}}_{\mathsf{f}}$ yield

$$\dot V = -\frac{d_\omega}{J}\bar r^2 - \frac{\kappa\lambda}{2}\big(\Gamma(\bar{\mathsf{y}}_{\mathsf{f}}) - \Gamma(0)\big)\bar{\mathsf{y}}_{\mathsf{f}} \le 0. \tag{48}$$

Since Γ is strictly increasing, $(\Gamma(\bar{\mathsf{y}}_{\mathsf{f}}) - \Gamma(0))\bar{\mathsf{y}}_{\mathsf{f}} = 0$ if and only if $\bar{\mathsf{y}}_{\mathsf{f}} = 0$. Hence $\dot V = 0$ if and only if $\bar r = 0$ and $\bar{\mathsf{y}}_{\mathsf{f}} = 0$. Let $\mathcal{M}$ be the largest invariant set contained in $\{(\bar\xi,\bar\mu) : \bar r = 0, \bar{\mathsf{y}}_{\mathsf{f}} = 0\}$. On $\mathcal{M}$, one has $\dot{\bar\mu} = k\bar r = 0$, $\bar\omega = v/\rho$, and $\dot{\bar s} = 2\bar x_e\bar r = 0$. Invariance of $\bar r = 0$ gives $0 = -(\rho/J)(\bar\mu - \mu^\star) - \kappa\Gamma(0)\psi'(\bar s)\bar x_e$. Since $\bar\mu$ and $\bar s$ are constant on $\mathcal{M}$, differentiating this identity along $\mathcal{M}$ yields $0 = -\kappa\Gamma(0)\psi'(\bar s)(v/\rho)(\bar y_e + \rho)$. Thus, $\bar y_e = -\rho$. Invariance of $\bar y_e = -\rho$ gives $\bar x_e = 0$, and the preceding identity gives $\bar\mu = \mu^\star$. Finally, $\bar{\mathsf{y}}_{\mathsf{f}} = 0$ and $\bar s = 0$ imply $\bar z = \psi(0)$. Therefore $\mathcal{M}$ is the singleton $(\xi^\star,\mu^\star)$. By the invariance principle, the equilibrium is globally attractive. Together with global stability, this proves global asymptotic stability. □

For each fixed $\epsilon > 0$, the closed-loop system (45) is forward complete: the constant forward speed keeps the vehicle position bounded on every finite time interval, and hence s, y_m, z, and $H(\mathsf{y}_\mathsf{f})$ remain bounded there, while (ω, μ) evolve according to a linear system driven by bounded inputs. By the symmetric product approximation [17], the solutions of (45) in the variables of (17) approximate the solutions of (46) on compact time intervals. In the terminology of Definition 1, we state the main result as a consequence of Proposition 3 and Lemma 1.

Theorem 2. *Suppose Assumption 1 holds. Choose the shaping function H such that (14) is satisfied. Then, the target point $(\xi^\star, \mu^\star)$ is semi-globally practically uniformly asymptotically stable for (45) in the variables of (17).*

Remark 2. The velocity-assisted design shows how the stability region can be enlarged when velocity measurements are available. The additional measurement of the yaw-rate tracking error allows the bias to be adjusted directly, instead of being tuned through the steady input–output map used in the output-feedback design. This removes the need to rely only on local exponential stability of the fixed-bias averaged dynamics. As a result, the averaged closed-loop system admits a global Lyapunov function. The conclusion for the original system remains semi-global and practical because it is obtained through averaging. Nevertheless, the result shows that the source-centered orbit can be practically stabilized from arbitrarily large prescribed compact sets without measuring the vehicle position, heading, source location, field gradient, inertia, or damping coefficient.

Remark 3. In practical implementations, the torque excitation a/ϵ should be selected with the available actuator range in mind. For a fixed a, this may limit how small ϵ can be, while reducing a decreases the required torque amplitude at the cost of a weaker averaged steering effect. The washout filter (12) is intended to remove the slowly varying component of the scalar measurement; when measurement noise is significant, additional filtering may be useful in implementation. A more detailed study of actuator constraints and measurement noise is left for future work. For practical tuning, δ is first decreased until the bias dither is sufficiently fast on the slow time scale, after which Ω is reduced to obtain adequate separation between the bias and plant dynamics. A smaller Ω improves this separation but slows the bias convergence, while a larger b increases both the averaged descent rate and the oscillatory bias-update amplitude. Finally, ϵ is reduced as needed to improve the fast-torque approximation, subject to the available actuator range. The filter rate λ may be chosen on the plant time scale, whereas k in the velocity-assisted design sets the aggressiveness of the bias adjustment.

5. Numerical simulations

This section illustrates the proposed torque-tuning designs through numerical simulations. All parameters are given in SI units. The source is placed at the origin, i.e., $(x^\star, y^\star) = (0, 0)$, and the scalar field is chosen as

$$\Phi(x, y) = \psi(x^2 + y^2), \tag{49}$$

where $\psi(s) := s$. The physical parameters are $J = 0.06$, $d_\omega = 0.12$, $\rho = 0.15$, and $v = 0.8$. Hence, $\mu^\star = d_\omega v/\rho = 0.64$.

For the output-feedback design (13), the controller parameters are selected as $a = 0.2$, $\epsilon = 0.02$, $b = 1$, $\Omega = 0.005$, $\delta = 0.2$, and $\lambda = 2$. For the velocity-assisted design (44), the parameters shared with the output-feedback design are kept the same, and the additional gain is selected as $k = 0.0015$. In both cases, $\mu(0) = 0.05$, and the washout filter is initialized as $z(0) = \mathsf{y}_\mathsf{m}(0)$. The excitation signals are chosen as $u_1(\sigma) = \cos(\sigma)$, $u_2(\sigma) = \sin(\sigma)$, and $w(\sigma) = \sin(\sigma)$, with $T = T_w = 2\pi$, which satisfy (9) and (10). The shaping function is $H(q) := 3e^{q/30}$, which satisfies (14). The initial vehicle state is $(x(0), y(0), \theta(0), \omega(0)) = (10, 10, 0, 0)$.

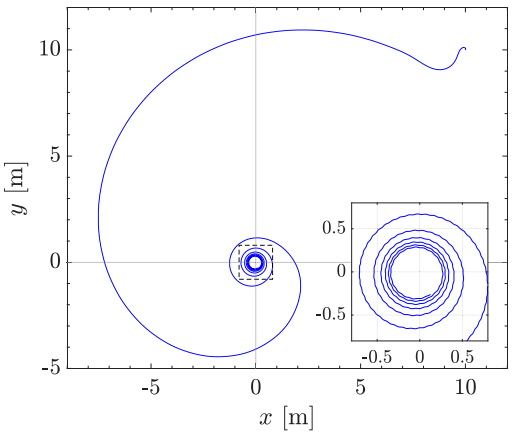


Fig. 3. Planar trajectory of the vehicle center under the output-feedback design (13). The source is located at the origin.

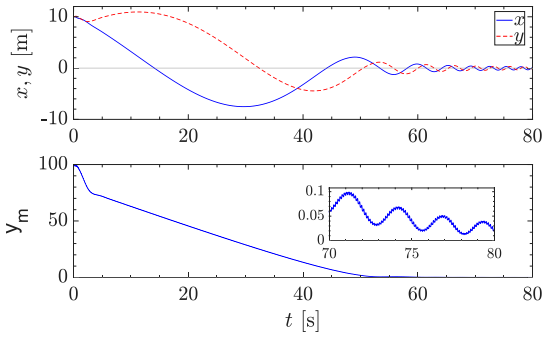


Fig. 4. Closed-loop position coordinates and scalar measurement under the output-feedback design (13).

Figs. 3 and 4 show the response under the output-feedback design (13). The vehicle center approaches a small orbit around the source, and the scalar measurement $\mathsf{y}_\mathsf{m}(t)$ decreases to a small neighborhood of zero. Although the theoretical guarantee for the output-feedback design is local, the simulation shows convergence from the relatively large initial condition $(x(0), y(0)) = (10, 10)$.

Figs. 5 and 6 show the response under the velocity-assisted design (44). Compared with the output-feedback design, the transient is shorter, and the vehicle reaches the source-centered orbit more directly. The scalar measurement also converges faster to a neighborhood of zero.

Fig. 7 uses a longer horizon to show the slow bias μ evolution. The dashed line denotes $\mu^\star$. The velocity-assisted design drives $\mu(t)$ toward $\mu^\star$, as predicted by the averaged analysis. The output-feedback design exhibits larger slow oscillations in $\mu(t)$, which is consistent with the Lie bracket bias-tuning mechanism.

6. Conclusion

This paper developed two torque-tuning source-seeking designs for a nonholonomic vehicle with a laterally displaced scalar sensor. A fast oscillatory torque input was used to generate an averaged steering effect through symmetric product approximation. For the output-feedback design, a slow Lie bracket bias update was introduced using only the real-time measurement $\mathsf{y}_\mathsf{m}(t)$, yielding local practical convergence under a nested selection of the tuning parameters. When measurements of v and ω are additionally available, the bias was tuned through the yaw-rate tracking error. This velocity-assisted design

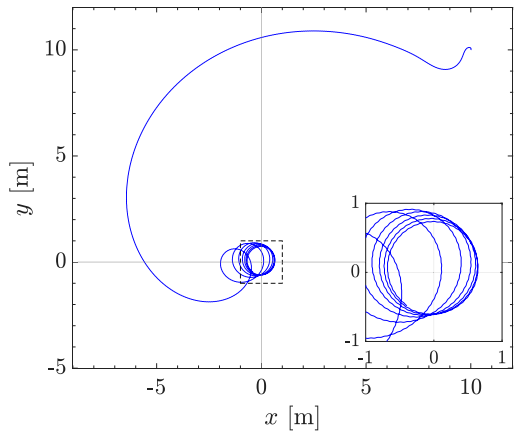


Fig. 5. Planar trajectory of the vehicle center under the velocity-assisted design (44). The source is located at the origin.

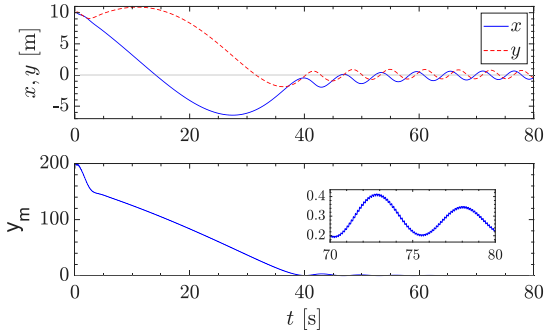


Fig. 6. Closed-loop position coordinates and scalar measurement under the velocity-assisted design (44).

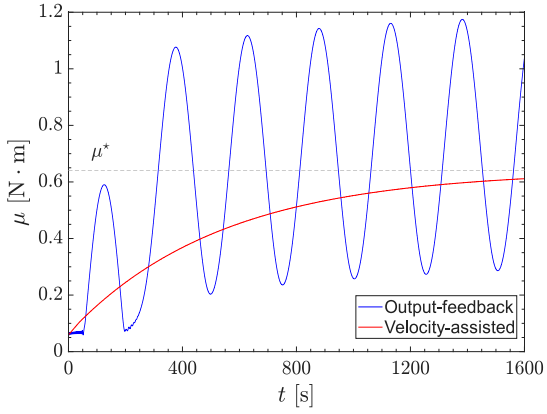


Fig. 7. Time histories of the yaw-torque bias $\mu(t)$ under the output-feedback and velocity-assisted designs. The dashed line denotes the nominal bias $\mu^\star = 0.64$.

yields a globally asymptotically stable averaged system and, consequently, semi-global practical uniform asymptotic stability for the original closed-loop system. Future work will address actuator saturation and experimental validation on robotic platforms.

Declaration of competing interest

The authors declare that they have no known competing financial interests or personal relationships that could have appeared to influence the work reported in this paper.

Data availability

No data was used for the research described in the article.

References

[1] M. Krstić, H.-H. Wang, Stability of extremum seeking feedback for general nonlinear dynamic systems, Automatica 36 (4) (2000) 595–601.
[2] K.B. Ariyur, M. Krstić, Real-Time Optimization by Extremum-Seeking Control, John Wiley & Sons, Hoboken, NJ, 2003.
[3] A. Scheinker, 100 years of extremum seeking: A survey, Automatica 161 (2024) 111481.
[4] C. Zhang, D. Arnold, N. Ghods, A. Siranosian, M. Krstić, Source seeking with non-holonomic unicycle without position measurement and with tuning of forward velocity, Syst. Control Lett. 56 (3) (2007) 245–252.
[5] C. Zhang, A. Siranosian, M. Krstić, Extremum seeking for moderately unstable systems and for autonomous vehicle target tracking without position measurements, Automatica 43 (10) (2007) 1832–1839.
[6] B. Wang, S. Nersesov, H. Ashrafiuon, P. Naseradinmousavi, M. Krstić, Underactuated source seeking by surge force tuning: Theory and boat experiments, IEEE Trans. Control Syst. Technol. 31 (4) (2023) 1649–1662.
[7] B. Wang, H. Ashrafiuon, S.G. Nersesov, Extremum seeking control for antenna pointing via symmetric product approximation, IFAC-PapersOnLine 59 (30) (2025) 869–874.
[8] A. Williams, A. Scheinker, E.-C. Huang, C. Taylor, M. Krstic, Experimental safe extremum seeking for accelerators, IEEE Trans. Control Syst. Technol. 32 (5) (2024) 1881–1890.
[9] P. Frihauf, S.-J. Liu, M. Krstic, A single forward-velocity control signal for stochastic source seeking with multiple nonholonomic vehicles, ASME J. Dyn. Syst. Meas. Contr. 136 (5) (2014) 051024.
[10] V. Todorovski, M. Krstić, Newton nonholonomic source seeking for distance-dependent maps, IEEE Trans. Autom. Control 70 (1) (2025) 510–517.
[11] J. Cochran, M. Krstić, Nonholonomic source seeking with tuning of angular velocity, IEEE Trans. Autom. Control 54 (4) (2009) 717–731.
[12] A. Raisch, M. Krstić, Overshoot-free steering-based source seeking, IEEE Trans. Control Syst. Technol. 25 (3) (2017) 818–827.
[13] H.-B. Dürr, M. Krstić, A. Scheinker, C. Ebenbauer, Extremum seeking for dynamic maps using Lie brackets and singular perturbations, Automatica 83 (2017) 91–99.
[14] N. Ghods, M. Krstić, Speed regulation in steering-based source seeking, Automatica 46 (2) (2010) 452–459.
[15] J. Lin, S. Song, K. You, C. Wu, 3-D velocity regulation for nonholonomic source seeking without position measurement, IEEE Trans. Control Syst. Technol. 24 (2) (2016) 711–718.
[16] P.C.S. Silva, P.C. Pellanda, T.R. Oliveira, Gradient-based stochastic extremum seeking for multivariable systems with distinct input delays, IEEE Trans. Autom. Control 71 (8) (2026) 5549–5556.
[17] F. Bullo, Averaging and vibrational control of mechanical systems, SIAM J. Control Optim. 41 (2) (2002) 542–562.
[18] R. Suttner, Extremum-seeking control for a class of mechanical systems, IEEE Trans. Autom. Control 68 (2) (2023) 1200–1207.
[19] R. Suttner, M. Krstić, Extremum seeking control for fully actuated mechanical systems on Lie groups in the absence of dissipation, Automatica 152 (2023) 110945.
[20] R. Suttner, Extremum seeking control for an acceleration controlled unicycle, IFAC-PapersOnLine 52 (16) (2019) 676–681.
[21] R. Suttner, M. Krstić, Acceleration-actuated source seeking without position and velocity sensing, IFAC-PapersOnLine 53 (2) (2020) 5348–5355.
[22] R. Suttner, M. Krstić, Source seeking with a torque-controlled unicycle, IEEE Control Syst. Lett. 7 (2023) 79–84.
[23] R. Suttner, M. Krstić, Nonholonomic source seeking in three dimensions using pitch and yaw torque inputs, Syst. Control Lett. 178 (2023) 105584.
[24] R. Suttner, M. Krstić, Nonlocal nonholonomic source seeking despite local extrema, IEEE Trans. Autom. Control 69 (4) (2024) 2575–2582.
[25] R. Suttner, M. Krstić, Overcoming local extrema in torque-actuated source seeking using the divergence theorem and delay, Automatica 167 (2024) 111799.
[26] L. Moreau, D. Aeyels, Practical stability and stabilization, IEEE Trans. Autom. Control 45 (8) (2000) 1554–1558.
[27] H.K. Khalil, Nonlinear Systems, third ed., Prentice-Hall, Upper Saddle River, NJ, 2002.
[28] H.-B. Dürr, M.S. Stanković, C. Ebenbauer, K.H. Johansson, Lie bracket approximation of extremum seeking systems, Automatica 49 (6) (2013) 1538–1552.